Journal of Alloys and Compounds 893 (2021) 162308

Contents lists available at ScienceDirect

Journal of Alloys and Compounds

journal homepage: www.elsevier.com/locate/jalcom

Remarkably stable high mobility self-aligned oxide TFT by investigating the effect of oxygen plasma time during PEALD of SiO_2 gate insulator

Seong-In Cho, Jong Beom Ko, Seung Hee Lee, Junsung Kim, Sang-Hee Ko Park*

Department of Materials Science and Engineering, Korea Advanced Institute of Science and Technology (KAIST), 291 Daehak-ro, Yuseong-gu, Daejeon 305-701, Republic of Korea

ARTICLE INFO

Article history:
Received 13 July 2021
Received in revised form 15 September 2021
Accepted 8 October 2021
Available online 13 October 2021

Keywords:
Oxide semiconductors
PEALD
Thin-film transistors
Oxygen plasma
High stability
High mobility

ABSTRACT

Oxide thin-film transistors (TFTs) should be manufactured with high mobility and stability based on a self-aligned top-gate structure to drive high-end displays. In this study, the effect of oxygen plasma time over one cycle of plasma-enhanced atomic layer deposition (PEALD) SiO_2 on the properties of top-gate oxide TFTs was investigated systemically. The subsurface reaction of oxygen plasma causes a difference in oxygen vacancy (V_o). In addition, hydrogen incorporation also differs according to plasma time. Considering V_o and hydrogen are donors, tendency of electric properties could be explained. These surface reactions and atomic incorporation also induce differences in the positive bias temperature stress (PBTS) stability. Based on oxygen plasma time of 2.0 s, a positive shift in threshold voltage (V_{th}) due to interfacial degradation was observed when the plasma was longer, while an abnormal negative shift due to H^+ drift was observed when it was shorter. When the oxygen plasma time is 2.0 s, the TFT was free from the deterioration of the interface and SiO_2. Based on this condition, a self-aligned TFT with superior performance including a high mobility of 31.1 cm^2/V s, positive V_{th} and high stability of 0.016 V shifting during the PBTS was fabricated successfully.

1. Introduction

Recently, thin-film transistors (TFTs) based on oxide semiconductors, known as oxide TFTs, have been evaluated as outstanding candidates for driving components of next-generation displays [1–3]. For a high-resolution, large-area display, the number of pixels that need to be driven at the same time increases, and uniformity becomes more important. From this point of view, the high mobility and uniformity of oxide TFTs perfectly satisfy these requirements. Since the sphere-shaped ns-orbitals of metals form electron transport paths, oxide semiconductors can maintain high mobility even in the amorphous phase [4]. To achieve these requirements, various types of high mobility oxide semiconductors, such as InO_x [5], InSnZnO (ITZO) [6,7], InZnO (IZO) [8], InGaZnO (IGZO) [9], and InGaSnO (IGTO) [10] have been researched. In addition, oxide semiconductors can be easily deposited by the sputtering method with high uniformity over a large area. Furthermore, the high transparency and flexibility of oxide semiconductors also make them suitable for use in next-generation displays [11,12]. Among the various types of oxide TFTs, self-aligned (SA) structured oxide TFTs have received considerable attention owing to their advantages, including reduction of resistive-capacitive (RC) delay by minimizing the parasitic capacitance [13–15]. The RC delay, which causes the kick-back effect, is another serious issue prevalent in high-resolution displays. This kick-back effect must be resolved because it induces an image sticking issue in the display. In the SA structure, the gate insulator (GI) is patterned using the gate electrode as a mask; thus, the overlap between the source & drain (S/D) electrode and gate electrode can be minimized, and parasitic capacitance, which is one of the reasons behind the RC delay, can be minimized. Therefore, a thinner GI can be applied to SA TFTs. For TFTs to have a higher on-current, thinner GIs must be used, which simultaneously increases the parasitic capacitance. Since SA TFT is relatively free from this issue, a thinner GI can be used in them compared to TFTs with other structures [16].

In addition to SA TFTs, numerous novel structured TFTs are based on a top-gate (TG) structure [17,18]. It is a challenging task to design an oxide TFT with the desired electrical properties for the TG structure. In particular, the GI deposition process should be carefully designed. Unlike the bottom-gate (BG) structure, an oxide semiconductor is exposed to the GI deposition process in the TG structure. During this process, the properties of the oxide semiconductor can be completely changed by an unavoidable doping reaction. In addition, the quality of the GI and interface between the GI and the active layer in which the channel is formed is also dominated by GI

* Corresponding author.
E-mail address: shkp@kaist.ac.kr (S.-H.K. Park).

https://doi.org/10.1016/j.jallcom.2021.162308
0925-8388/

deposition. Even though the same materials and structures except GI deposition are employed, considerable differences in the electrical properties and stability of oxide TFTs can be observed [16,19,20]. An excellent solution for these issues is GI deposited by plasma-enhanced atomic layer deposition (PEALD). Although there are several reports on oxide TFTs with PEALD process GI showing good positive bias temperature stress (PBTS) stability [7,16,19,20], the GI deposition parameters of PEALD still need to be carefully designed.

In this study, we investigated the effect of oxygen plasma time over one cycle of PEALD of SiO_2, which is one of the parameters of the PEALD process. First, we analyzed the effect of oxygen plasma time during PEALD on the electrical characteristics and stability of top-gate bottom-contact (TGBC) structured oxide TFTs. In addition, the cause of this effect was identified through various material analyses and electrical measurements. Finally, considering these effects comprehensively, we successfully fabricated extremely stable high mobility SA structured oxide TFTs by applying the optimized oxygen plasma time for one cycle of PEALD.

2. Experimental section

2.1. Fabrication of TGBC oxide TFTs based on PEALD of SiO_2 with different oxygen plasma times

To mimic the material stack and fabrication process of the SA TFT, TGBC-structured oxide TFTs based on PEALD of SiO_2 were fabricated (Fig. 1(a)). First, InSnO (ITO) deposited on a glass substrate was employed as the S/D electrode. Then, 20 nm Al-doped InSnZnO (Al:ITZO) was deposited by RF sputtering at 25 °C under a 40% oxygen partial pressure. Next, the samples were annealed at 350 °C for 2 h under an oxygen atmosphere. Then, 20 nm thick SiO_2 was deposited at 300 °C by PEALD with different oxygen plasma times. Fig. 1(b) shows one cycle of PEALD of SiO_2. Bisdiethylamino silane (BDEAS, $H_2Si[N(C_2H_5)_2]_2$) and 100 W of oxygen plasma were used as the precursors for Si and oxygen, respectively. We split this oxygen plasma time into 0.3, 2.0, and 4.0 s. Next, 180 nm of plasma-enhanced chemical vapor deposition (PECVD) SiO_2 was deposited at 300 °C. SiH_4 and 75 W of N_2O plasma were used as reactants for Si and oxygen during the PECVD process. Finally, an 80 nm thick Mo layer was deposited by DC sputtering. All thin films were patterned using photolithography and wet etching. After fabrication, vacuum annealing at 340 °C was performed for 2 h. The width and length of the active layer were 20 and 10 μm, respectively.

2.2. Fabrication of a highly stable high mobility SA oxide TFT based PEALD of SiO_2

First, 20 nm Al:ITZO of the active layer was deposited by RF sputtering at 25 °C on a Si wafer with thermal oxide. The partial oxygen pressure was set at 40%. Then, the sample was annealed under oxygen atmosphere at 350 °C for 2 h. Next, 20 nm of PEALD SiO_2, the first GI, was deposited directly on Al:ITZO at 300 °C. The oxygen plasma time over one cycle of PEALD was 2.0 s, which was optimized for TGBC oxide TFTs. Similar to the fabrication process of the TGBC oxide TFT, BDEAS and 100 W of oxygen plasma were used as the Si and oxygen precursors, respectively. Then, 80 nm thick PECVD SiO_2 was deposited at 300 °C, and 80 nm thick Mo was deposited by DC sputtering. Next, vacuum annealing was conducted at 340 °C for 2 h. In the TGBC structure, the vacuum annealing was conducted after all the processes were completed. In contrast, in the SA structure, the annealing process was conducted after the gate electrode deposition, which was followed by the subsequent processes. This yields the incorporations of an optimized amount of H from the GI into the Al:ITZO in the TGBC structure, preventing H flowing from other layers such as interlayer dielectric (ILD). After vacuum annealing, the Mo gate electrode was patterned by photolithography and wet etching, and then, the exposed SiO_2 was dry etched using the gate electrode as a mask for the SA structure. Next, Ar plasma treatment (100 W for 60 s at 200 °C) was conducted on the exposed Al:ITZO to form the n^+ S/D contact region. Then, 100 nm of PECVD SiO_2 for the ILD was deposited at 270 °C. The ILD pattern was also formed through dry etching. Finally, 100 nm thick Mo was deposited by DC sputtering for the S/D electrode. The width and length of the Al:ITZO films were 20 and 10 μm, respectively.

2.3. Electrical measurements and characterizations

The electrical properties of the oxide TFTs were measured using HP4156A under ambient conditions. The bias stress to the gate electrode was 1 MV/cm (20 V for TGBC oxide TFTs and 10 V for SA oxide TFTs), and the temperature stress was 60 °C under PBTS conditions. The bias stresses to the gate and drain electrodes during the current stress stability (CSS) measurement were 4 and 4.5 V, respectively. The carrier concentration of Al:ITZO was measured using Hall measurements (HL5500PC). X-ray photoelectron spectroscopy (XPS) (K-alpha) was conducted to analyze the differences in the transfer curves and SiO_2 thin films under each condition. Additionally, to determine the H-related component of the thin film, secondary ion mass spectroscopy (SIMS) (IMS7f) was conducted. The densities of the SiO_2 thin films were compared using X-ray reflectometry (XRR) (SmartLab). In addition, the quantitative H amount of plasma-enhanced atomic layer deposited SiO_2 according to the oxygen plasma time was determined by elastic recoil detection (ERD) (NFC). The imaginary dielectric function (ε_2), which is associated with the electron trap site in the thin film, was extracted using spectroscopic ellipsometer (SE) (M2000D) analysis. To analyze the bonding state of plasma-enhanced atomic layer deposited SiO_2, Fourier transform-infrared (FT-IR) spectra (IF66V/S) were obtained.

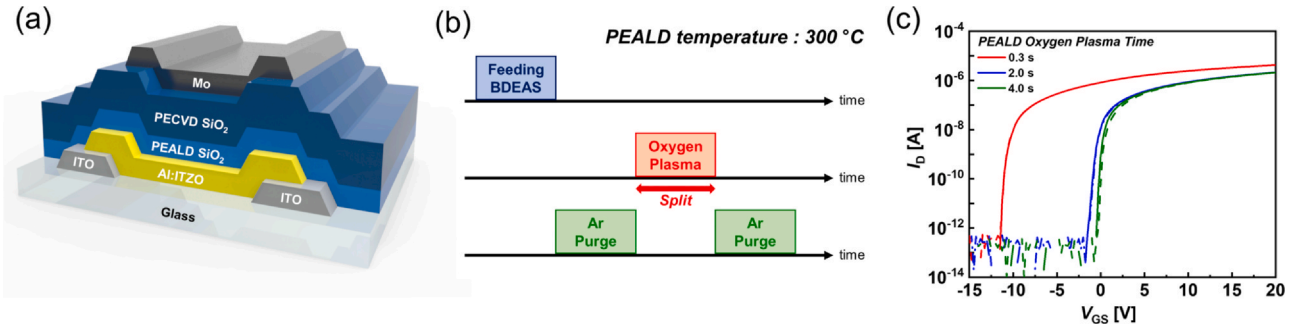

Fig. 1. Schematic diagram of (a) the TGBC oxide TFT with PEALD SiO_2 and (b) sequence of one cycle of PEALD of SiO_2. (c) Transfer curves of oxide TFTs with different oxygen plasma times during PEALD (V_{DS} = 0.1 V). Solid lines show forward sweeps, and dashed lines show back sweeps.

3. Result and discussion

3.1. Effect of oxygen plasma time for PEALD of SiO_2 on the electrical properties of the top-gate Al:ITZO TFTs

Fig. 1(a) shows the structure and materials of the oxide TFT fabricated using PEALD SiO_2, which forms an interface with Al:ITZO. As shown in Fig. 1(b), the oxygen plasma time over one cycle of PEALD of SiO_2 was split into 0.3, 2.0, and 4.0 s. Except for this parameter, all materials and fabrication processes remained constant. Fig. 1(c) shows the transfer curves of the three oxide TFTs fabricated using PEALD with different oxygen plasma times, and the electrical characteristics extracted from the transfer curves are summarized in Table 1. A simple change in the parameter of GI deposition led to dramatic differences in the electrical characteristics, including mobility and threshold voltage (V_{th}). As the plasma time increased, the V_{th} value changed to a proper positive value from −6.38 to 1.69 V; however, the mobility decreased relatively from 46.50 to 32.52 cm^2/V s. The device fabricated using PEALD with an oxygen plasma time of 0.3 s exhibited the highest mobility, but showed an excessively negative V_{th} value, which is not suitable for display-driving applications. In contrast, when the longest plasma deposition time (4.0 s) was used, a slight clockwise hysteresis remained, even though annealing was performed. The clockwise hysteresis occurs due to the defects at the interface between the GI and active layer [21]. The defects at the interface trap electrons and serve as a negative voltage, which results in clockwise hysteresis. All three oxide TFTs showed high mobility over 30 cm^2/V s.

Because of the unique energy band structure of the oxide semiconductor, both mobility and V_{th} depend on the carrier concentration of the oxide semiconductor [12]. Considering the electrical properties of the fabricated oxide TFTs according to the oxygen plasma time, it becomes essential to analyze how the oxygen plasma used in the deposition of the GI affects the characteristics of the Al:ITZO, especially in terms of the carrier concentration and formation of trap site. In fact, Hall measurements showed that the oxygen plasma time of this PEALD process has a significant effect on the carrier concentration of Al:ITZO (Fig. 2). Because the fabrication processes including photolithography and deposition of Hall measurement samples were all the same as those of the TFT fabrication, analyzing the device characteristics is useful. Al:ITZO fabricated with 0.3 s of oxygen plasma time during SiO_2 deposition showed a much higher carrier concentration (2.35×10^{18} cm^{-3}) than others. Comparing the cases of 2.0 (1.25×10^{17} cm^{-3}) and 4.0 s (5.87×10^{16} cm^{-3}) oxygen plasma times, we found that the shorter the plasma time, the higher the carrier concentration of Al:ITZO.

A possible approach for changing the carrier concentration according to the GI deposition parameter is the difference in the oxygen vacancy (V_o) of Al:ITZO. In fact, V_o is a well-known shallow donor for oxide semiconductors [4,22]. To determine the V_o concentration of Al:ITZO according to the SiO_2 deposition conditions, XPS depth profiles were obtained. Direct PEALD of SiO_2 was performed on Al:ITZO, similar to device fabrication, and the O1s peak of Al:ITZO at the interface was investigated. The O1s peak of Al:ITZO was deconvoluted into metal-oxygen bonding (M-O, 529.68 eV), V_o (530.98 eV), and oxygen–hydrogen or carbon bonding (O-H or O-C, 532.15 eV), and their portions were extracted from the peak area [16]. As shown in Fig. 3, the V_o concentration of Al:ITZO increased as the oxygen plasma time of GI deposition decreased from 12.40% to 29.22%, as the oxygen plasma time of PEALD decreased. In fact, when the plasma time was short, a shoulder was observed in the O1s peak, indicating that the V_o concentration and carrier concentration of Al:ITZO varied depending on the GI deposition conditions. The carrier concentration of Al:ITZO without SiO_2 was 6.27×10^{20} cm^{-3} according to the Hall measurement, which is higher than the carrier concentration of Al:ITZO with SiO_2; this indicated that the effect of oxygen plasma during PEALD was quite significant. This supports reactive oxygen plasma generated during PEALD filled the V_o sites in the active layer effectively, similar to the oxygen plasma treatment. In fact, several studies have reported that oxygen plasma treatment changes the V_o concentration of the oxide semiconductor [16,23]. Although no separate oxygen plasma treatment to the active layer was performed in our experiment, the oxygen plasma used for SiO_2 deposition could have sufficiently induced an effect similar to that of oxygen plasma treatment to change the properties of Al:ITZO, due to its TG structure.

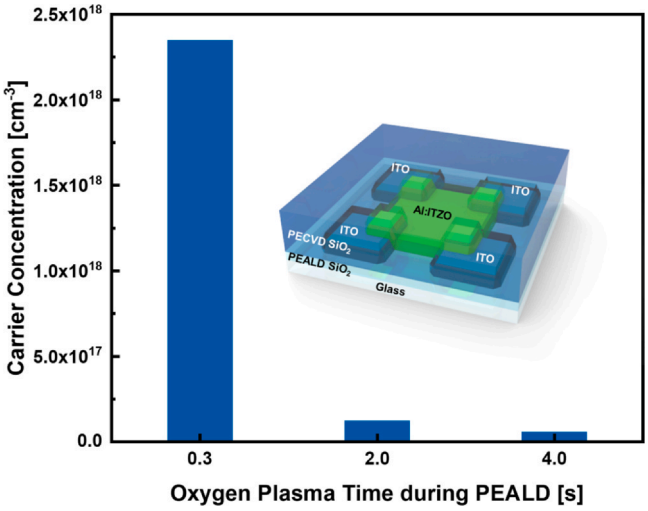

Fig. 2. Carrier concentration of Al:ITZO with PEALD SiO_2 and PECVD SiO_2 from Hall measurement.

When considering the order of deposition of materials, the atomic incorporation during PEALD can also be a factor causing the difference in the carrier concentration. In fact, when H contained in the BDEAS precursor is incorporated, it can act as a donor [7,13,16]. Furthermore, external H may diffuse into the Al:ITZO during the post-annealing process. To analyze the H-related element distribution in the SiO_2/Al:ITZO stack, SIMS was conducted. Fig. 4(a) and (b) show the distribution of the H and OH elements after the annealing process. When oxygen plasma was applied for a short time, more H and OH elements in Al:ITZO were observed. This difference in the number of H-related components in Al:ITZO already exists before the annealing process due to the incorporated H during PEALD (Fig. S1). However, the difference in the number of H atoms in Al:ITZO becomes more apparent due to diffuse in or out of H during the annealing process. Considering that incorporated H is also a shallow donor of oxide semiconductors, the difference in carrier concentration could be due to H in addition to V_o [22,24]. Two main sources of this difference in incorporated H can be considered: (1) The density of PEALD SiO_2 differs according to the oxygen plasma time, and thus the inflow of H from the outside differs. (2) When the concentration of H in PEALD SiO_2 itself varies depending on the oxygen plasma time, the amount of H diffused into Al:ITZO from PEALD SiO_2 also becomes different. To check the possibility of the H source in the first case, the density of the PEALD SiO_2 thin film was analyzed using

Table 1
Electrical characteristics of oxide TFTs with different oxygen plasma times during PEALD.

PEALD oxygen plasma time	0.3 s	2.0 s	4.0 s
Field-effect mobility [cm^2/V s]	46.50	35.91	32.52
Subthreshold swing [V/decade]	0.22	0.23	0.13
Hysteresis [V]	0	0	0.21
V_{th} [V]	-6.38	1.16	1.69

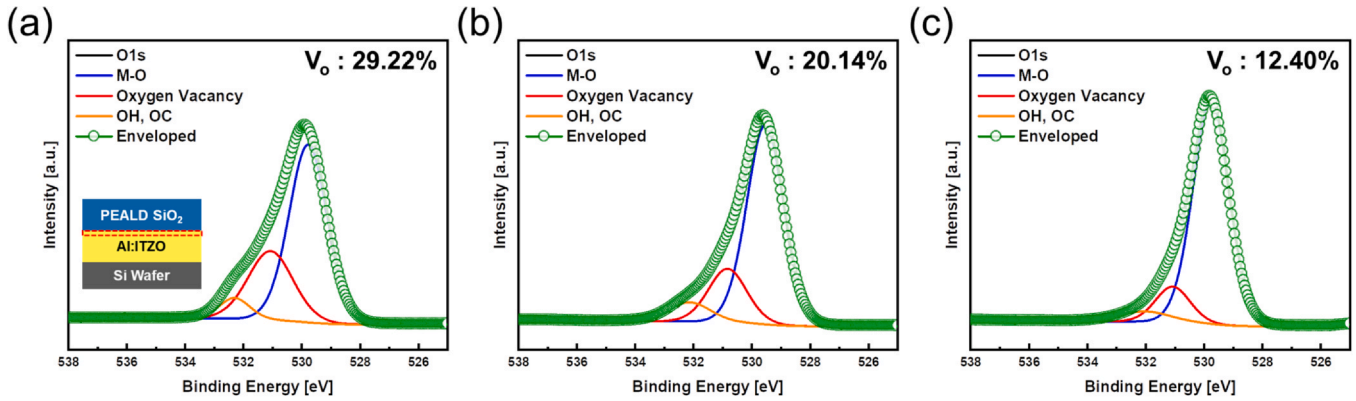

Fig. 3. O1s peaks from the XPS depth profile results of Al:ITZO with an SiO_2 layer fabricated using PEALD at oxygen plasma times of (a) 0.3, (b) 2.0, and (c) 4.0 s.

XRR. Fig. 4(c) displays the XRR data of the plasma-enhanced atomic layer deposited SiO_2 thin films. The density of the thin film was determined using the critical angle at which the intensity begins to decrease. When the three SiO_2 thin films were compared by expanding the region near the critical angle, SiO_2 deposited at oxygen plasma times of 2.0 and 4.0 s showed almost the same graph. In the case of oxygen plasma time of 0.3 s, the intensity began to decrease at slightly lower angles than the cases of 2.0 and 4.0 s oxygen plasma times. This implies that there is little difference in density when the oxygen plasma times are 2.0 and 4.0 s, and when the oxygen plasma time is 0.3 s, the density is slightly lower than that in the cases of 2.0 and 4.0 s. Considering the XRR results, it is difficult to state that the difference in the amount of H in Al:ITZO that was confirmed using SIMS is due to the difference in SiO_2 density. In the case of 0.3 s oxygen plasma time, which had the highest H in Al:ITZO, the density was relatively low; however, it is difficult to say that it causes a large difference in the amount of H in Al:ITZO. In addition, even in the case of 2.0 and 4.0 s, the H concentration in Al:ITZO differed, but no difference was observed in the density of PEALD SiO_2. In contrast, the second possible H source was confirmed by quantitatively analyzing the amount of H in the PEALD SiO_2 through ERD. Fig. 4(d)–(f) show the amount of H in the PEALD SiO_2 thin film under each case of oxygen plasma time. SiO_2 deposited using the shortest oxygen plasma time of 0.3 s contained the highest amount of H (6.32×10^{16} atoms/cm^2). In contrast, SiO_2 deposited under oxygen plasma times of 2.0 and 4.0 s had an H amount of 3.13×10^{16} and 1.79×10^{16} atoms/cm^2, respectively. This shows that the difference in H content between PEALD SiO_2 thin films is almost two or three times larger and can explain the tendency observed in the SIMS analysis. SiO_2 deposited with a shorter oxygen plasma time contains more H, which can be incorporated into Al:ITZO during PEALD and followed post-processing. Some of the incorporated H acts as a donor, affecting the electrical properties of the TFTs. This trend of H concentration observed through ERD can be easily understood through the mechanism of PEALD. The incomplete reaction between the BDEAS and oxygen plasma during PEALD generate residual impurities including

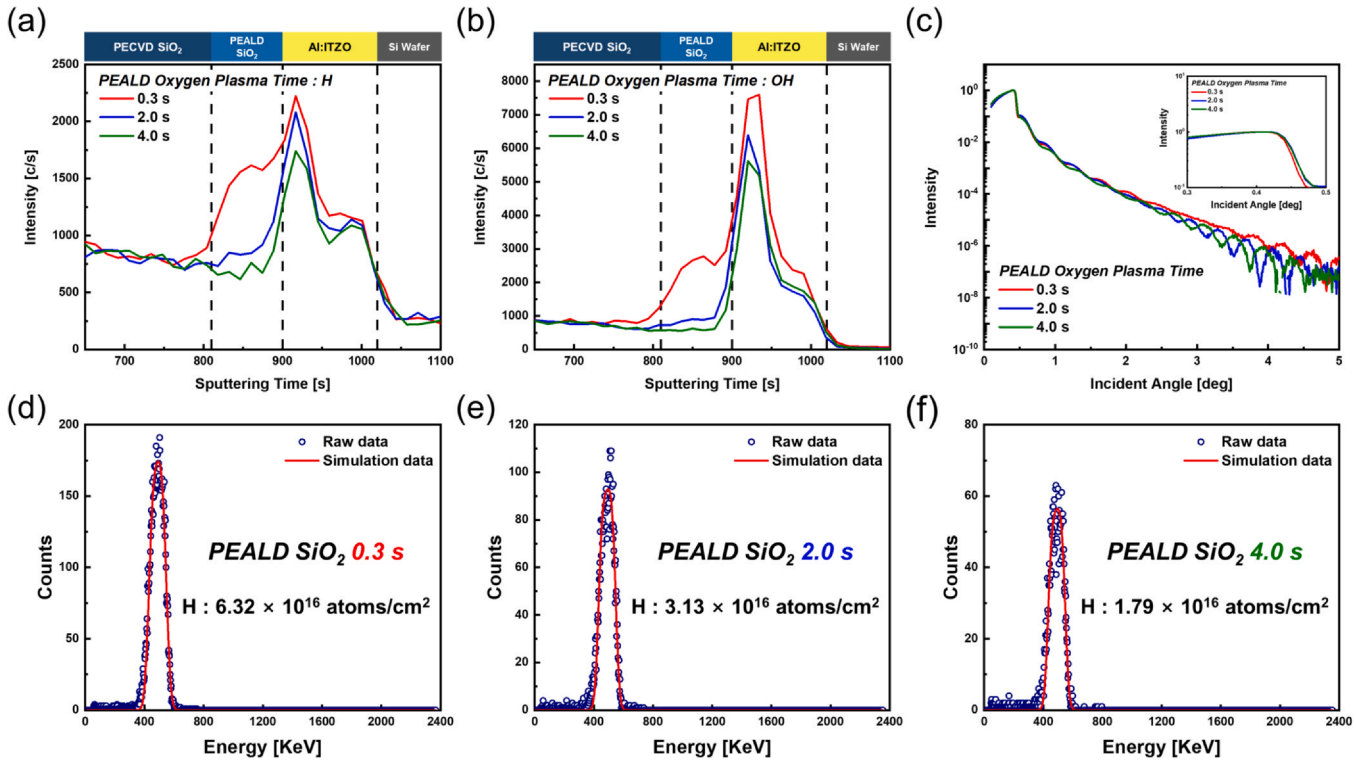

Fig. 4. Distribution of (a) H and (b) OH elements in the SiO_2/Al:ITZO material stack as measured by SIMS analysis after 340 °C vacuum annealing. (c) Result of XRR analysis of PEALD SiO_2 thin films. Quantitative amount of H in PEALD SiO_2 thin film fabricated under oxygen plasma times of (d) 0.3, (e) 2.0, and (f) 4.0 s measured by ERD.

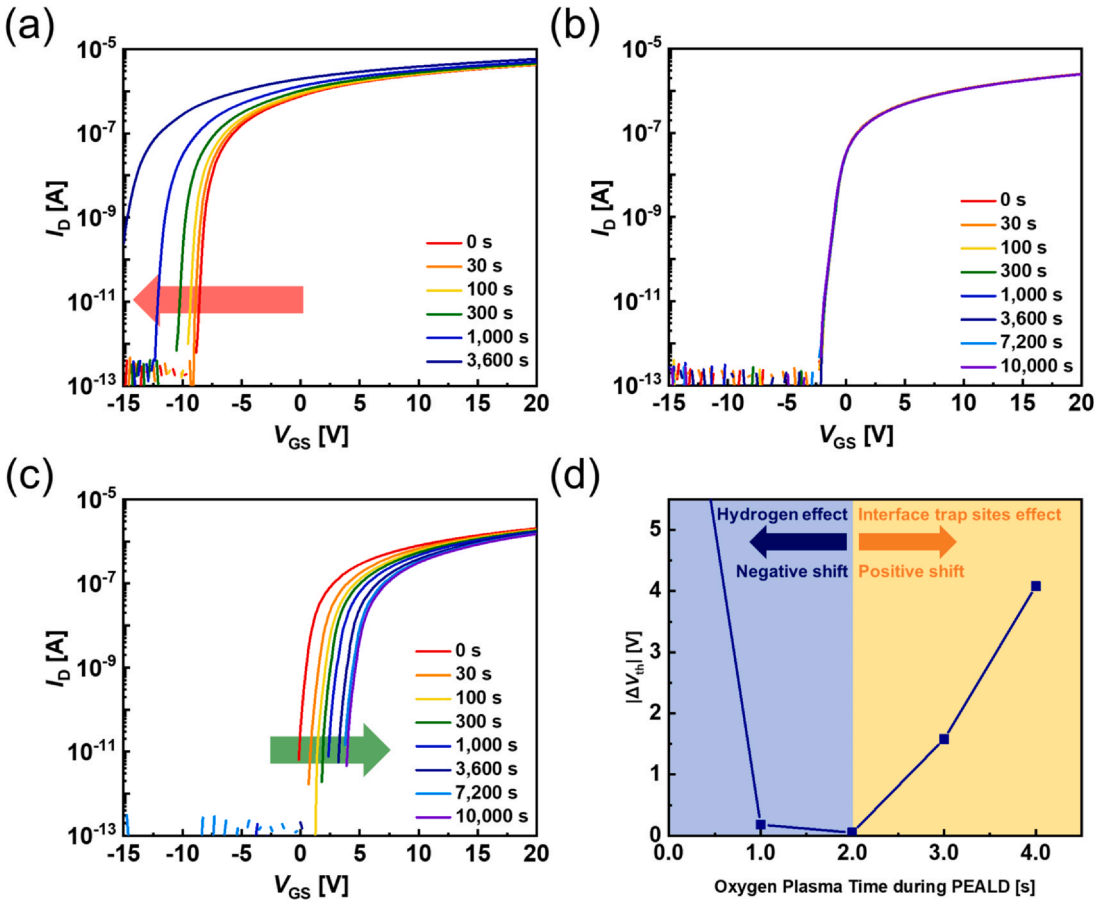

Fig. 5. Transfer curves of oxide TFTs under PBTS condition over 10,000 s during PEALD with different oxygen plasma times of (a) 0.3, (b) 2.0, and (c) 4.0 s (d) PBTS stability results for all oxygen plasma times.

H from the precursor remain in the thin film [25–27]. In this experiment, the oxygen plasma time is the variable determining the reactivity of the precursor, where the short oxygen plasma time reduces the reactivity between BDEAS and oxygen plasma, thereby leading to a higher residual H concentration.

3.2. PBTS stability of top-gate Al:ITZO TFTs according to oxygen plasma time during PEALD of SiO_2

The electrical characteristics as well as the stability of Al:ITZO TFTs with PEALD SiO_2 changed dramatically according to the oxygen plasma time during PEALD. Fig. 5(a)–(c) show the results of the PBTS stability of oxide TFTs with oxygen plasma times of 0.3, 2.0, and 4.0 s. To clarify the trend according to the plasma time, the PBTS stability of the oxide TFTs fabricated using oxygen plasma times of 1.0 and 3.0 s were also measured (Fig. S2). The trend of PBTS stability results is presented in Fig. 5(d). Based on the reliability of the oxide TFT optimized with the oxygen plasma time is 2.0 s, a peculiar tendency was observed. The transfer curve moved in the positive direction under the PBTS condition when the plasma time was longer than 2.0 s. Meanwhile it moved in the negative direction when it was shorter than 2.0 s. In contrast, at 2.0 s, the transfer curve hardly moved over 10,000 s, showing excellent PBTS stability. In general, PBTS instability is caused by the electron-trapping mechanism in defects within the GI bulk and interface between GI and active layer [27,28]. In this case, the trapped electrons act as a negative gate bias, causing the transfer curves to move in the positive direction. However, because this measurement of PBTS stability showed different trends around oxygen plasma time of 2.0 s, to analyze this trend, it was necessary to separate and analyze the effect of oxygen plasma time during PEALD of longer and shorter than 2.0 s on PBTS stability.

To understand the trend of PBTS stability over 2.0 s, CSS measurements were conducted. CSS can evaluate whether the driving TFT can maintain a constant brightness by passing a constant current to the light emitting element of a current-driven display. The result of CSS measurement also deteriorates when the oxygen plasma time increases by greater than 2.0 s, which is the same as the trend observed for PBTS stability. At an oxygen plasma time of 2.0 s, 98.45% current was maintained after 1 h; however, only 88.69% and 84.51% current values were maintained at oxygen plasma times of 3.0 and 4.0 s, respectively. The current decay can be fitted with the stretched exponential equation as follows:

$$\frac{I_D(t)}{I_D(0)} = exp\left\{-\left(\frac{t}{\tau}\right)^{\beta}\right\}$$

where $I_D(t)$ and $I_D(0)$ are the drain current at time t and the initial state (t = 0), respectively. β indicates the dispersion parameter, which describes the trap distribution, and τ is directly correlated with the mean time of electrons to be in the mobile state [16,29,30]. The blue, orange, and green lines shown in Fig. 6(a) are results that fit the CSS measurement results of 2.0, 3.0, and 4.0 s β and τ values extracted from the fitted stretched exponential equation are compiled in Table 2. The results of CSS measurements match well with the stretched exponential model, suggesting that the dominant mechanism of these instabilities is charge trapping at the defect sites [29,30]. To determine the origin of electron capture sites related to oxygen plasma, SE analysis was performed on a single SiO_2 thin film. Fig. 6(b) shows the ε_2 extracted from the SE analysis versus the

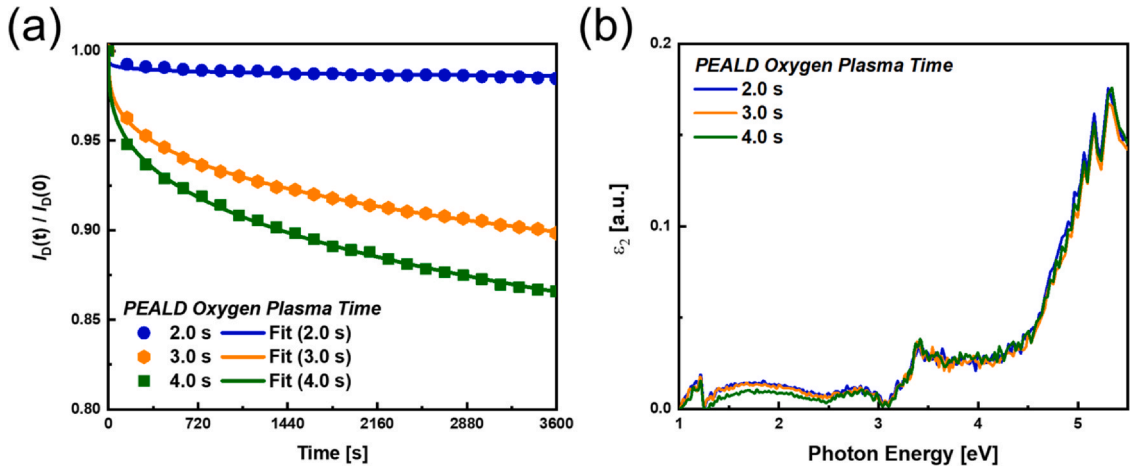

Fig. 6. (a) Results of current stress stability during 3600 s of TFTs under oxygen plasma times of 2.0, 3.0, and 4.0 s during PEALD of SiO_2. (b) Spectroscopic ellipsometer results of SiO_2 thin films fabricated with different oxygen plasma times. (For interpretation of the references to color in this figure legend, the reader is referred to the web version of this article.)

Table 2
Extracted τ and β values from CSS measurements.

PEALD oxygen plasma time	2.0 s	3.0 s	4.0 s
τ [s]	8.42×10^{18}	4.67×10^{6}	1.30×10^{6}
β	0.12	0.31	0.33

photon energy. ε_2 is correlated with the electron-trapping sites inside the SiO_2 thin film [31]. The results of SE analysis show that there is no significant difference in the defects in the SiO_2 thin film according to the oxygen plasma time. This SE result agrees well with the previously mentioned XRR data. From the XRR results, it was confirmed that there is almost no difference in the density of PEALD SiO_2 under 2.0 and 4.0 s oxygen plasma times. The density of thin films is strongly related to the number of defects in the thin film [19,32]. No difference in density between SiO_2 plasma-enhanced atomic layer deposited under 2.0 and 4.0 s oxygen plasma times implies that the number of defects in the SiO_2 is also not significantly different, which is the same as results obtained from the SE data. This implies that the electron-trapping sites present at the interface between SiO_2 and Al:ITZO, rather than inside SiO_2, degrade the stability. In fact, oxygen plasma generates defects such as oxygen interstitials (O_i) and dangling bonds at the interface of oxide semiconductors, and these O_i and dangling bonds are well known as electron trap sites [33,34]. The longer the oxygen plasma time, the more O_i and dangling bonds are generated, which is thought to be the reason for the degradation in stability when the plasma time exceeds 2.0 s. In addition, the reduction in the H concentration of SiO_2 can also be considered as a factor responsible for stability deterioration. The SIMS and ERD results were mentioned earlier, and only the role of H as a donor was mentioned. However, H can also act as a defect passivator [24,27]. As mentioned before, the H concentration decreases along with the increased oxygen plasma time as shown in Fig. 4(e) and (f). While the number of defects that should be passivated increases due to the increase oxygen plasma time, the concentration of H as a defect passivator decreases to yield poor stability.

When a short 0.3 s oxygen plasma time was used for GI deposition, an abnormal shift in the negative direction of the transfer curve was observed under PBTS conditions. In this case, the instability cannot be explained by the electron-trapping mechanism. Jeong et al. reported a similar negative shift phenomenon of the transfer curve under PBTS conditions from SiO_2 GI-based oxide TFTs, similar to the device used in this study [19]. They explained this phenomenon by H^+ incorporation from the H-rich SiO_2 GI under PBTS condition. The authors explained that the H atoms present in SiO_2 in the form of OH drift into the oxide semiconductor in the form of H^+ under a positive gate voltage (V_{GS}). These incorporated H atoms during PBTS operation act as donors and cause a negative shift in V_{th}.

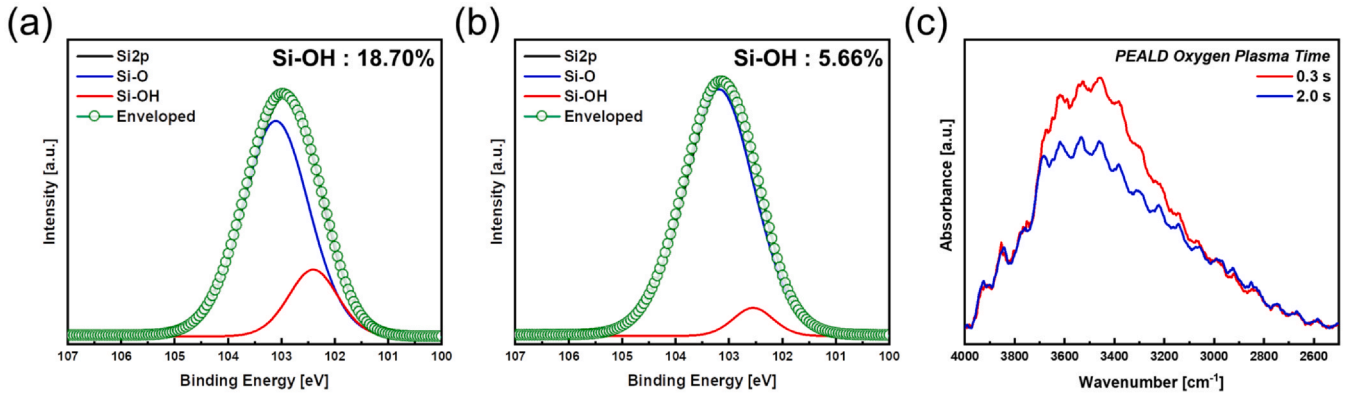

Fig. 7. Si2p peaks and deconvoluted peaks from XPS analysis of SiO_2 films fabricated under oxygen plasma times of (a) 0.3 and (b) 2.0 s using PEALD. (c) FT-IR spectroscopy of plasma-enhanced atomic layer deposited SiO_2 under different oxygen plasma times.

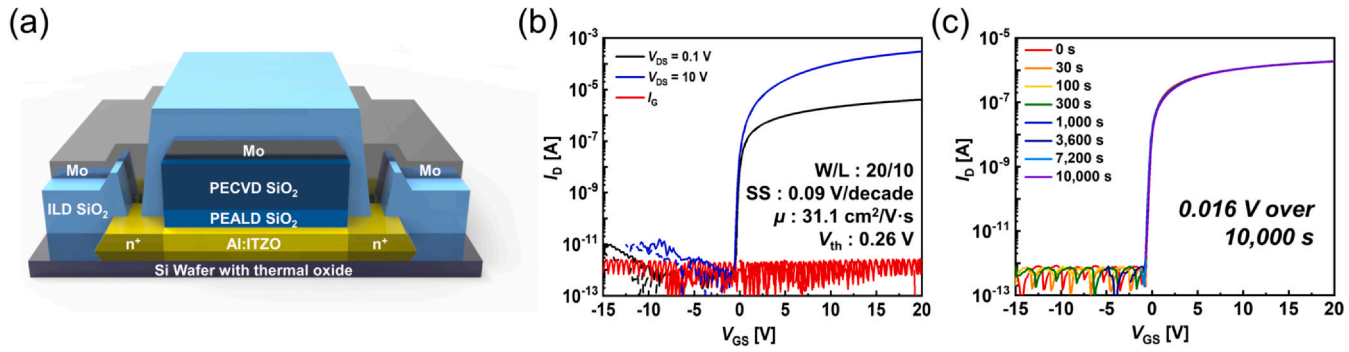

Fig. 8. (a) Schematic diagram of the fabricated SA oxide TFT. (b) Transfer curves of SA oxide TFT under an oxygen plasma time of 2.0 s during PEALD of SiO_2. Solid lines show forward sweeps and dashed lines show back sweeps. (c) Transfer curves of SA oxide TFT under PBTS condition over 10,000 s (V_{DS} = 0.1 V).

Considering that the H concentration in the SiO_2 thin film under an oxygen plasma of 0.3 s was higher than that of other films in the previous ERD data (Fig. 4(d)–(f)), the bonding state of H was investigated through XPS and FT-IR spectra to confirm the applicability of this H incorporation mechanism to this device. Fig. 7(a) and (b) show the Si2p peaks of PEALD SiO_2 under oxygen plasma times of 0.3 and 2.0 s, respectively. Each Si2p peak is deconvoluted into Si–O (103.15 eV) and Si–OH (102.48 eV) sub-peaks [19,35]. SiO_2 deposited under a 0.3 s oxygen plasma time has a higher Si–OH bonding portion of 18.70% than that deposited under a 2.0 s oxygen plasma time (5.66%), relatively. This bonding state was also confirmed by the FT-IR spectra. SiO_2 deposited under an oxygen plasma time of 0.3 s showed a higher intensity of the Si–OH peak, presented at the wavenumber of 2750–3600 cm^{-1} [19,36]. This result matches the previous ERD and XPS data very well and is similar to the result reported by Jeong et al. [19]. A satisfactory surface chemical reaction does not occur during the PEALD process of SiO_2 because the oxygen plasma time is short, and more H atoms remain in the SiO_2 thin film. Some of these H atoms exist in the form of OH and are incorporated into the Al:ITZO under PBTS conditions in the form of H^+ and act as donors [19,37]. This instability is due to the deterioration of the SiO_2 thin film. Conversely, when a sufficient oxygen plasma time of 2.0 s was used, high quality SiO_2 was deposited and stability degradation due to H^+ drift did not occur. This indicates that even if a gate electrode with a high work function or oxide semiconductor with a low carrier concentration is used to shift V_{th} to a proper value, it is difficult to apply PEALD SiO_2 deposited with a very short oxygen plasma time to a display driving application [38,39].

We observed that the optimal time for oxygen plasma is 2.0 s, in which neither interfacial deterioration due to electron capture sites nor degradation of the insulator due to the high H concentration is 2.0 s. Owing to these properties, a high mobility, acceptable V_{th}, and excellent stability were observed.

3.3. Remarkably stable high mobility, self-aligned Al:ITZO TFT based on PEALD SiO_2 with optimized oxygen plasma time

Fig. 8(a) shows a schematic diagram of the fabricated SA oxide TFT with optimized oxygen plasma time of 2.0 s over one cycle of PEALD. The detailed process differs from that used to fabricate the TGBC structure. However, the active layer, GI, and the interface between them, which dominate the electrical properties and stability of the device, are designed to be the same as those of the TGBC structure. The transfer curve of the SA Al:ITZO TFT is shown in Fig. 8(b). The SA oxide TFT also showed high mobility over 30 cm^2/V s, and other electrical characteristics, including V_{th} and subthreshold swing (SS), were also excellent. The result of the PBTS stability of the SA oxide TFT based on PEALD SiO_2 with an optimized oxygen plasma time of 2.0 s is shown in Fig. 8(c). Owing to the high quality of the active layer, GI, and the interface between them, which were previously optimized by oxygen plasma time during PEALD, SA oxide TFT showed excellent stability with only a shift of 0.016 V over 10,000 s

Table 3 summarizes the structure and characteristics of the previously reported oxide TFTs. Compared to previously reported devices, the best results were observed in all respects. Considering the suitable SA structure for display driving and the relatively short channel length, the SA oxide TFT reported in this study shows remarkable performance in terms of mobility and stability. In addition, the turn-on voltage is very close to 0 V. Therefore, the fabricated SA

Table 3
Comparison of the stability and mobility among the previously reported oxide TFTs and the SA oxide TFT fabricated in this study.

Active / GI	Structure	Mobility [cm^2/V s]	Length [μm]	PBTS (PBS) stability [V]	Ref.
ZnO / AlO_x	BGTC	35.36	10	0.15 (3600 s)	[40]
ZnO / SiO_2	BGTC	4.5	100	4.25 (1000 s)	[41]
ZnO & In_2O_3 / SiO_2	BGTC	36	50	1.1 (86,400 s)	[42]
IZO / Al_2O_3	BGBC	14.40	250	1.97 (7200 s)	[43]
IZO / SiO_2	BGTC	8.1	100	1.5 (3600 s)	[44]
IGZO / Al_2O_3	TGBC	15.1	20	1.8 (10,000 s)	[45]
IGZO / Al_2O_3	TGBC	9.65	20	0.98 (10,000 s)	[46]
IGZO / SiO_2	BGTC	30.3	20	< 0.5 (3600 s)	[9]
IGZO / SiO_2	Self-Aligned	9.0	10	0.2 (3600 s)	[15]
IGZO / HfO_2	TG	–	–	< 1 (10,000 s)	[47]
IGZO:H / SiO_2	BGTC	26.5	120	2.5 (3600 s)	[24]
ITZO / SiO_2	BGTC	68.5	–	1.1 (3600 s)	[7]
ITZO / SiO_2	TGBC	21.11	40	2.87 (3600 s)	[19]
ITZO / $ZrSiO_x$	BGTC	28.6	20	0.64 (3600 s)	[6]
Al:ITZO / Al_2O_3	TGBC	35.3	20	0.23 (10,000 s)	[16]
IGZTO / SiO_2	BGTC	46.7	300	0.5 (3600 s)	[48]
LiGdZnO / ZrO_x	BGTC	25.87	10.03	0.05 (3600 s)	[49]
Al:ITZO / SiO_2	Self-Aligned	31.1	10	0.016 (10,000 s)	This work

oxide TFT is highly suitable for driving various electronics including displays. These remarkable results could be achieved because the device has been optimized by analyzing the changes in the quality and interfacial properties of the thin films according to the oxygen plasma time, a parameter of PEALD of SiO_2.

4. Conclusion

We investigated the effect of oxygen plasma time over one cycle of PEALD of SiO_2. By optimizing this parameter, a remarkably stable high mobility SA oxide TFT was successfully fabricated. Because SiO_2 was directly deposited on the Al:ITZO active layer owing to its TG structure, the oxygen plasma time had a dominant effect on the quality of SiO_2, the properties of Al:ITZO, and the interface between them, causing changes in the device characteristics for various reasons. The difference in the carrier concentration of Al:ITZO according to the oxygen plasma time caused the differences in electrical properties, including mobility and V_{th}. XPS depth profile and SIMS analysis showed that the PEALD oxygen plasma time difference caused a V_o concentration change of Al:ITZO and the modulation of the amount of incorporated H. In addition, the stability of PBTS dramatically changed according to the oxygen plasma time during PEALD. When the plasma time was longer than 2.0 s, a positive shift in the transfer curve was observed based on the electron-trapping mechanism. The long oxygen plasma time during GI deposition generated O_i and dangling bonds at the interface, thereby degrading the stability of the TFTs. When the oxygen plasma time was too short, a negative shift of the transfer curve was observed based on the H incorporation mechanism. A very short oxygen plasma time increased the amount of OH in the SiO_2 thin film, and H^+ drifted into the Al:ITZO under the positive V_{GS} to act as a shallow donor. When the oxygen plasma time was 2.0 s, it was free from interfacial degradation and SiO_2 deterioration, thus high mobility and high stability characteristics were secured. The SA structured oxide TFT fabricated under an oxygen plasma time of 2.0 s showed a high mobility of 31.1 $cm^2/V{\cdot}s$ and an excellent PBTS stability of only 0.016 V shifting over 10,000 s. This is remarkable even when compared with previously reported studies that considered display applications.

CRediT authorship contribution statement

Seong-In Cho: Conceptualization, Methodology, Investigation, Formal analysis, Investigation, Visualization, Writing – original draft, Writing – review & editing. **Jong Beom Ko:** Conceptualization, Methodology, Investigation, Validation. **Seung Hee Lee:** Methodology, Investigation. **Junsung Kim:** Methodology, Investigation. **Sang-Hee Ko Park:** Supervision, Resources, Project administration, Funding acquisition, Writing – review & editing.

Declaration of Competing Interest

The authors declare that they have no known competing financial interests or personal relationships that could have appeared to influence the work reported in this paper.

Acknowledgment

This work was supported by the Samsung Display Corporation through the KAIST Samsung Display Research Center Program. This work was also supported by a National Research Foundation of Korea (NRF) grant funded by the Korean government (MSIT) (2018R1A2A3075518).

Appendix A. Supporting information

Supplementary data associated with this article can be found in the online version at doi:10.1016/j.jallcom.2021.162308.

References

[1] J.S. Park, W.J. Maeng, H.S. Kim, J.S. Park, Review of recent developments in amorphous oxide semiconductor thin-film transistor devices, Thin Solid Films 520 (2012) 1679–1693.
[2] D. Ji, J. Jang, J.H. Park, D. Kim, Y.S. Rim, D.K. Hwang, Y.Y. Noh, Recent progress in the development of backplane thin film transistors for information displays, J. Inf. Disp. 22 (2021) 1–11.
[3] E. Fortunato, P. Barquinha, R. Martins, Oxide semiconductor thin-film transistors: a review of recent advances, Adv. Mater. 24 (2012) 2945–2986.
[4] T. Kamiya, K. Nomura, H. Hosono, Origins of high mobility and low operation voltage of amorphous oxide TFTs: electronic structure, electron transport, defects and doping, J. Disp. Technol. 5 (2009) 273–288.
[5] H.I. Yeom, J.B. Ko, G. Mun, S.H.K. Park, High mobility polycrystalline indium oxide thin-film transistors by means of plasma-enhanced atomic layer deposition, J. Mater. Chem. C 4 (2016) 6873–6880.
[6] M. Kim, H.J. Jeong, J. Sheng, W.H. Choi, W. Jeon, J.S. Park, The impact of plasma-enhanced atomic layer deposited ZrSiOx insulators on low voltage operated In-Sn-Zn-O thin film transistors, Ceram. Int. 45 (2019) 19166–19172.
[7] J.Z. Sheng, J.H. Han, W.H. Choi, J. Park, J.S. Park, Performance and stability enhancement of In-Sn-Zn-O TFTs using SiO2 gate dielectrics grown by low temperature atomic layer deposition, ACS Appl. Mater. Interfaces 9 (2017) 42928–42934.
[8] D.C. Paine, B. Yaglioglu, Z. Beiley, S. Lee, Amorphous IZO-based transparent thin film transistors, Thin Solid Films 516 (2008) 5894–5898.
[9] J. Sheng, T. Hong, H.M. Lee, K. Kim, M. Sasase, J. Kim, H. Hosono, J.S. Park, Amorphous IGZO TFT with high mobility of similar to 70 cm(2)/(V s) via vertical dimension control using PEALD, ACS Appl. Mater. Interfaces 11 (2019) 40300–40309.
[10] B.K. Kim, N. On, C.H. Choi, M.J. Kim, S. Kang, J.H. Lim, J.K. Jeong, Polycrystalline indium gallium tin oxide thin-film transistors with high mobility exceeding 100 cm(2)/Vs, IEEE Electron Device Lett. 42 (2021) 347–350.
[11] T. Kamiya, H. Hosono, Material characteristics and applications of transparent amorphous oxide semiconductors, Npg Asia Mater. 2 (2010) 15–22.
[12] T. Kamiya, K. Nomura, H. Hosono, Present status of amorphous In-Ga-Zn-O thin-film transistors, Sci. Technol. Adv. Mater. 11 (2010).
[13] W. Jeong, J. Winkler, H. Schmidt, K.H. Lee, S.H.K. Park, Suppressing channel-shortening effect of self-aligned coplanar Al-doped In-Sn-Zn-O TFTs using Mo-Al alloy source/drain electrode as Cu diffusion barrier, J. Alloy. Compd. 859 (2021) 158227.
[14] D.H. Kang, I. Kang, S.H. Ryu, J. Jang, Self-aligned coplanar a-IGZO TFTs and application to high-speed circuits, IEEE Electron Device Lett. 32 (2011) 1385–1387.
[15] H.Y. Jeong, S.H. Nam, K.S. Park, S.Y. Yoon, C. Park, J. Jang, Significant performance and stability improvements of low-temperature IGZO TFTs by the formation of In-F nanoparticles on an SiO(2)buffer layer, Nanomaterials 10 (2020).
[16] J.B. Ko, S.H. Lee, K.W. Park, S.H.K. Park, Interface tailoring through the supply of optimized oxygen and hydrogen to semiconductors for highly stable top-gate-structured high-mobility oxide thin-film transistors, RSC Adv. 9 (2019) 36293–36300.
[17] C.S. Hwang, S.H.K. Park, H. Oh, M.K. Ryu, K.I. Cho, S.M. Yoon, Vertical channel ZnO thin-film transistors using an atomic layer deposition method, IEEE Electron Device Lett. 35 (2014) 360–362.
[18] H.J. Joo, M.G. Shin, S.H. Kwon, H.Y. Jeong, H.S. Jeong, D.H. Kim, X.S. Jin, S.H. Song, H.I. Kwon, High-gain complementary inverter based on corbino p-type tin monoxide and n-type indium-gallium-zinc oxide thin-film transistors, IEEE Electron Device Lett. 40 (2019) 1642–1645.
[19] S.G. Jeong, H.J. Jeong, W.H. Choi, K. Kim, J.S. Park, Hydrogen impacts of PEALD InGaZnO TFTs using SiOx gate insulators deposited by PECVD and PEALD, IEEE Trans. Electron Devices 67 (2020) 4250–4255.
[20] J.B. Ko, H.I. Yeom, S.H.K. Park, Plasma-enhanced atomic layer deposition processed SiO2 gate insulating layer for high mobility top-gate structured oxide thin-film transistors, IEEE Electron Device Lett. 37 (2016) 39–42.
[21] Z. Ye, Y.G. Yuan, H. Xu, Y. Liu, J.K. Luo, M. Wong, Mechanism and origin of hysteresis in oxide thin-film transistor and its application on 3-D nonvolatile memory, IEEE Trans. Electron Devices 64 (2017) 438–446.
[22] K. Ide, K. Nomura, H. Hosono, T. Kamiya, Electronic defects in amorphous oxide semiconductors: a review, Phys. Status Solidi A 216 (2019) 1800372.
[23] S. Yang, K.H. Ji, U.K. Kim, C.S. Hwang, S.H.K. Park, C.S. Hwang, J. Jang, J.K. Jeong, Suppression in the negative bias illumination instability of Zn-Sn-O transistor using oxygen plasma treatment, Appl. Phys. Lett. 99 (2011) 102103.
[24] A. Abliz, Effects of hydrogen plasma treatment on the electrical performances and reliability of InGaZnO thin-film transistors, J. Alloy. Compd. 831 (2020) 154694.
[25] M. Putkonen, M. Bosund, O.M.E. Ylivaara, R.L. Puurunen, L. Kilpi, H. Ronkainen, S. Sintonen, S. Ali, H. Lipsanen, X.W. Liu, E. Haimi, S.P. Hannula, T. Sajavaara, I. Buchanan, E. Karwacki, M. Vaha-Nissi, Thermal and plasma enhanced atomic layer deposition of SiO2 using commercial silicon precursors, Thin Solid Films 558 (2014) 93–98.

[26] A. Kobayashi, N. Tsuji, A. Fukazawa, N. Kobayashi, Temperature dependence of SiO2 film growth with plasma-enhanced atomic layer deposition, Thin Solid Films 520 (2012) 3994–3998.
[27] Y. Nam, H.O. Kim, S.H. Cho, S.H.K. Park, Effect of hydrogen diffusion in an In-Ga-Zn-O thin film transistor with an aluminum oxide gate insulator on its electrical properties, RSC Adv. 8 (2018) 5622–5628.
[28] A. Suresh, J.F. Muth, Bias stress stability of indium gallium zinc oxide channel based transparent thin film transistors, Appl. Phys. Lett. 92 (2008) 033502.
[29] W.H. Lee, S.J. Lee, J.A. Lim, J.H. Cho, Printed In-Ga-Zn-O drop-based thin-film transistors sintered using intensely pulsed white light, RSC Adv. 5 (2015) 78655–78659.
[30] S. Singh, Y.N. Mohapatra, Bias stress effect in solution-processed organic thin-film transistors: evidence of field-induced emission from interfacial ions, Org. Electron. 51 (2017) 128–136.
[31] C.S.P.G. Bersuker, J. Price, P. Lysaght, P. Krsch, R. Jammy, Nanoscale gate stacks: from atomic defects to device performance, E.S.C.Trans. (2009).
[32] S.M. Heald, B. Nielsen, Density and defects in thin metal-films using X-Ray reflectivity and variable-energy positrons, J. Appl. Phys. 72 (1992) 4669–4673.
[33] J. Sheng, J. Park, D.W. Choi, J. Lim, J.S. Park, A study on the electrical properties of atomic layer deposition grown InOx on flexible substrates with respect to N2O plasma treatment and the associated thin-film transistor behavior under repetitive mechanical stress, ACS Appl. Mater. Interfaces 8 (2016) 31136–31143.
[34] H.H. Nahm, Y.S. Kim, D.H. Kim, Instability of amorphous oxide semiconductors via carrier-mediated structural transition between disorder and peroxide state, Phys. Status Solidi B 249 (2012) 1277–1281.
[35] P. Post, L. Wurlitzer, W. Maus-Friedrichs, A.P. Weber, Characterization and applications of nanoparticles modified in-flight with silica or silica-organic coatings, Nanomaterials 8 (2018).
[36] A. Mirabedini, S.M. Mirabedini, A.A. Babalou, S. Pazokifard, Synthesis, characterization and enhanced photocatalytic activity of TiO2/SiO2 nanocomposite in an aqueous solution and acrylic-based coatings, Prog. Org. Coat. 72 (2011) 453–460.
[37] Y.C. Chien, Y.C. Yang, Y.C. Tsao, H.C. Chiang, M.C. Tai, Y.L. Tsai, P.H. Chen, T.M. Tsai, T.C. Chang, Hydrogen as a cause of abnormal subchannel formation under positive bias temperature stress in a-InGaZnO thin-film transistors, IEEE Trans. Electron Device 66 (2019) 2954–2959.
[38] W.J. Jang, M.K. Lee, J. Yoo, E. Kim, D.Y. Yang, J. Park, J.W. Park, S.H.K. Park, K.C. Choi, Low-resistive high-work-function gate electrode for transparent a-IGZO TFTs, IEEE Trans. Electron Devices 64 (2017) 164–169.
[39] J.S. Park, J.K. Jeong, Y.G. Mo, H.D. Kim, C.J. Kim, Control of threshold voltage in ZnO-based oxide thin film transistors, Appl. Phys. Lett. 93 (2008) 033513, https://doi.org/10.1063/1.2963978
[40] J.K. Saha, R.N. Bukke, N.N. Mude, J. Jang, Remarkable stability improvement of ZnO TFT with Al2O3 gate insulator by yttrium passivation with spray pyrolysis, Nanomaterials 10 (2020) 976.
[41] L.J. Wan, F.C. He, Y. Qin, Z.H. Lin, J. Su, J.J. Chang, Y. Hao, Effects of interfacial passivation on the electrical performance, stability, and contact properties of solution process based ZnO thin film transistors, Materials 11 (2018) 1761.
[42] Y.H. Lin, W. Li, H. Faber, A. Seitkhan, N.A. Hastas, D. Khim, Q. Zhang, X.X. Zhang, N. Pliatsikas, L. Tsetseris, P.A. Patsalas, D.D.C. Bradley, W. Huang, T.D. Anthopoulos, Hybrid organic-metal oxide multilayer channel transistors with high operational stability, Nat. Electron. 2 (2019) 587–595.
[43] M. Li, W. Zhang, W.F. Chen, M.L. Li, W.J. Wu, H. Xu, J.H. Zou, H. Tao, L. Wang, M. Xu, J.B. Peng, Improving thermal stability of solution-processed indium zinc oxide thin-film transistors by praseodymium oxide doping, ACS Appl. Mater. Interfaces 10 (2018) 28764–28771.
[44] H. Park, Y. Nam, J. Jin, B.S. Bae, Improvement of bias stability of oxyanion-incorporated aqueous sol-gel processed indium zinc oxide TFTs, J. Mater. Chem. C 2 (2014) 5998–6003.
[45] S.J. Yoon, N.J. Seong, K. Choi, W.C. Shin, S.M. Yoon, Investigations on the bias temperature stabilities of oxide thin film transistors using In-Ga-Zn-O channels prepared by atomic layer deposition, RSC Adv. 8 (2018) 25014–25020.
[46] K.W. Park, G. Jeon, S. Lee, J.B. Ko, S.H.K. Park, Effects of hydroxyl group in AlOx gate insulator on the negative bias illumination instability of In-Ga-Zn-O thin film transistors, Phys. Status Solidi A 216 (2019) 1800737.
[47] S.N. Choi, S.M. Yoon, Effects of oxidants on the bias-stress instabilities of In-Ga-Zn-O thin film transistors using HfO2 gate insulator prepared by atomic layer deposition, IEEE Electron Device Lett. 41 (2020) 425–428.
[48] I. Choi, M.J. Kim, N. On, A. Song, K.B. Chung, H. Jeon, J.K. Park, J.K. Jeong, Achieving high mobility and excellent stability in amorphous In-Ga-Zn-Sn-O thin-film transistors, IEEE Trans. Electron Devices 67 (2020) 1014–1020.
[49] J.K. Saha, R.N. Bukke, J. Jang, Extremely stable, high performance Gd and Li alloyed ZnO thin film transistor by spray pyrolysis, Adv. Electron. Mater. 6 (2020) 2000594.